Geodyn Algorithm

The GEODYN algorithm was described in a series of reports written by the Radio Science Working Group in Phase B. The main description is contained in the following memo:

RQ36 Asteroid Gravity Field and Rotation State Science Report

To: RSWG
From: Jay W. McMahon
Date: 10/30/12

Summary:
This memo provides a detailed, system-level description of the main algorithms and data types used for carrying out the Radio Science (RS) scientific measurement goals during the close proximity phase of the OSIRIS-REx mission.

Memo:
The Radio Science Working Group (RSWG) is tasked with determining the gravity field and rotation state of RQ36 through requirements 2.7.2 – 2.7.5 and 2.8.2 – 2.8.4. This memo outlines processing methodology, data acquisition strategy, and data products used to meet these requirements. Due to the fact that the determination of the gravity field and the rotation state of RQ36 are intrinsically linked, the discussions of both have been combined here.

<u>Processing Methodology</u>

The Radio Science (RS) team will use a software suite to estimate the required parameters through a linear least-squares parameter estimation problem. In this case, the system can be described by the equations,

$$\dot{\mathbf{x}} = A\mathbf{x}$$
$$\mathbf{y} = H\mathbf{x} + \epsilon$$

where x is the system state, A is the linearized dynamics matrix, y is the measurement vector, H is the linearized measurement matrix, and ε is the measurement error vector. The actual parameters and measurements that make up the state and measurement vectors will vary between different mission phases – the details of this will be discussed below.

Note that in reality, our system is non-linear, and therefore the state and measurement vectors shown above (x and y) are actually deviations from the reference trajectory values. The vector x is truly the state deviation vector,

$$\mathbf{x} = \mathbf{X} - \mathbf{X}^*$$

where X is the full non-linear state, and X* is the non-linear state on the reference trajectory. The vector y is the observation residual, which is the actual (observed) measurement minus the computed measurement from the reference trajectory at that time.

At the start of our operations (in DRM phase 4A), the current navigation team solution will be used as our reference trajectory. As operations progress, both the navigation solution and the previous RS solution can be used as a priori reference trajectories.

The maximum likelihood/minimum variance estimate of the state deviation, x, for a linear system is found by solving the weighted least-squares problem. This problem can be stated in the normal form as

$$\Lambda \hat{\mathbf{x}} = \mathbf{N}$$

where $\mathbf{\Lambda}$ is the information matrix, N is the normal vector, and the hat signifies the best estimate of the state, x. The information matrix and normal vector are given by

$$\Lambda = \sum_{i=1}^{N} \left[\widetilde{H}_i \Phi(t_i, t_0) \right]^T R_i^{-1} \widetilde{H}_i \Phi(t_i, t_0) + \bar{P}_0^{-1}$$

$$\mathbf{N} = \sum_{i=1}^{N} \left[\widetilde{H}_i \Phi(t_i, t_0) \right]^T R_i^{-1} \mathbf{y}_i + \bar{P}_0^{-1} \bar{\mathbf{x}}_0$$

where $\mathbf{\Phi}$ is the state transition matrix from time t_0 to time t_i, H-tilde is the linearized measurement matrix at time t_i, R_i is the measurement noise covariance matrix of the measurement at time t_i, P_0-bar is the a priori covariance matrix, and x_0-bar is the a priori state estimate. The state transition matrix is determined by propagation of the reference trajectory with the a priori values of all parameters over the duration of the arc. It is used in the previous equations to map the measurement information to the epoch time, t_0.

The RS process executes this as a batch filter, so that the summation of all observations over an entire arc is made, and then the best estimate is simply determined by inverting the normal equation. One further modification is made in that, for numerical stability, we solve this process through a Square-root Information Filter. This means that an orthogonal transformation is applied to the normal equation, resulting in a new equation of the form

$$S\hat{\mathbf{x}} = b$$

where S is an upper triangular matrix, so that the estimate can be solved for by backwards substitution, removing the need to take the inverse of the information matrix. This is computationally advantageous and more numerically stable than a regular information filter. Finally, the estimate of the non-linear state is updated as

$$\hat{\mathbf{X}} = \mathbf{X}^* + \hat{\mathbf{x}}$$

Due to the non-linear nature of this system, this process must be iterated with an updated reference trajectory until satisfactory convergence is reached. A flow chart of the estimation process is shown in Figure 1. The process described in this section is shown in blue. The inputs to this process (shown in yellow) will be discussed in the following section on the RS Data Acquisition Strategy, and the outputs (shown in green) are discussed in the Data Products section.

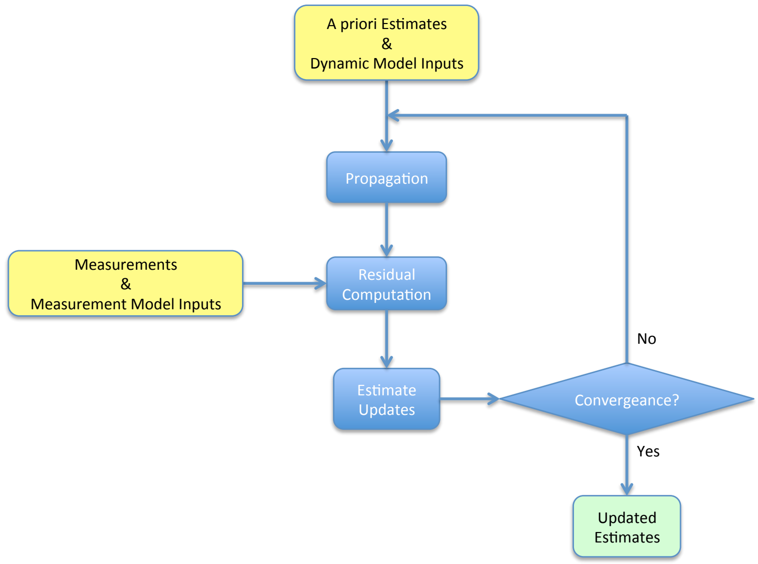

Figure 1 - Flow chart of the RS estimation process

A key component of implementing this process successfully is having a realistic and accurate dynamic model. The RS dynamic model will always include point mass gravity from RQ36 and solar radiation pressure. At the start of the RS mission, in DRM phase 4A, the information for this model will be limited, and these may be the only components. However, as the mission progresses and more information is gained, the RS model will include a gravity field up to at least 4^{th} degree and order, and the rotation state of RQ36. Depending on the length of the arc being processed, other perturbations such as tidal perturbations from the Sun may also be included, although this will likely only be done in post-processing. The parameters to be estimated, or the state, will follow this pattern of increasing complexity as with the dynamic model. The RS team is tasked with estimating the gravity field up to 4^{th} degree and order and the rotation state of RQ36, so these parameters, at a minimum, will be included in the state vector.

At this time, the nominal software package to execute the RS estimation process is Geodyn. This software has a long heritage in Earth orbiting missions, and is being modified for the needs of the RSWG. A detailed discussion of the usage of Geodyn for RS can be found in Reference 1.

Data Acquisition Strategy

The data acquisition strategy is driven by the DRM phases. There are two types of information required to execute the RS process: the inputs to the measurement and dynamic models, which are provided by groups outside of RS; second, the measurements that are used in the RS process to estimate the states. The RS process uses observations obtained from the DSN, as well as pre-processed measurements from the Altimetry and Optical Imaging working groups. In the following we discuss the inputs used throughout the mission, the measurements types used, and the cadence of acquiring the observations.

Inputs:

The dynamic models require all data pertaining to spacecraft dynamic activities, which are contained in the Spacecraft E kernel (spacecraft events) and the C Kernel (attitude information). As previously mentioned, the RS process can also be run with either a previous RS SP Kernel (state estimate solution) or a FDS SP Kernel as the a priori guess.

Measurement model inputs revolve around calibration data for the measurement instruments. Mainly this will be data delivered by the DSN including Earth orientation parameters, tracking station locations, and media calibration data. There will also be different parameters for each of the three X-band communications antennas (High-gain, medium-gain, and low-gain) on the spacecraft. Finally, this may also include calibration data for the spacecraft instruments such as the optical cameras (Polycam and Mapcam) and the LiDAR (OLA and/or the GNC LiDAR), depending on the specific measurements used for these items – see the discussion below.

Measurement Types:

The main measurement type for the RS estimation process is the radiometric ranging and Doppler signals obtained from the DSN. Ranging data actually measures the time it takes for a signal to travel between the spacecraft and the Earth, which can be related to the range between the observing station and the spacecraft by the speed of light,

$$\rho = \tau c$$

where ρ is the slant range, τ is the signal transit time, and c is the speed of light. The slant range provides information about the geocentric range because the station location is known.

The Doppler signal measures the change in the received signal frequency (f_R) from the transmitted signal frequency (f_T)

$$f_R = \left(1 - \frac{\dot{\rho}}{c}\right) f_T$$

Comparison of these frequencies reveals the slant range rate, $\dot{\rho}$, which causes the change in frequencies known as the Doppler shift. Note that for a round trip measurement, the Doppler shift is doubled, resulting in

$$f_R = \left(1 - \frac{2\dot{\rho}}{c}\right) f_T$$

The Doppler signal provides information on the spacecraft's geocentric range rate, $\dot{r}$, declination, δ, and right ascension, α, through the relationship

$$\dot{\rho} = \dot{r} + \omega_e r_s \cos\delta \sin(\omega_e t + \phi + \lambda_s - \alpha)$$

where ω_e is the Earth's rotation rate, r_s is the distance of the station from the Earth's spin axis, λ_s is the station longitude, ϕ is the right ascension of the mean Sun, and t is the universal time. An illustration of the Doppler signal is shown in Figure 2. The Doppler signal can also provide range information through the Doppler count which keeps track of the phase change between the received and sent signals; the phase change is related to the range change over the count period by the wavelength of the signal.

The ranging measurements can be one-way, two-way, or three-way. One-way ranging means that a signal is generated on-board the spacecraft and received by a DSN station. Two-way ranging has a DSN station transmit a signal, which is received by the spacecraft and sent back to the same DSN station. This is the preferred ranging methodology as it removes any synchronization issues between the spacecraft and ground clocks that corrupt the measurement as in one-way ranging. Finally, three-way ranging has one DSN station send a signal, which is turned around by the spacecraft, and received by a different DSN station. Three-way ranging is less accurate than two-way due to the fact that the signal does not make an exact round trip and two different ground clocks are used, but can be necessary to use in certain viewing geometries where two-way is not possible.

Due to the fact that the DSN measurements provide data with respect to the observing station, it is necessary to obtain data over long arcs and from multiple stations so that the viewing geometry changes over time. This helps to ensure that there aren't unobservable components of the spacecraft state. For example, an arc of range and Doppler data provide information about the position and velocity components normal to the geocentric radius vector.

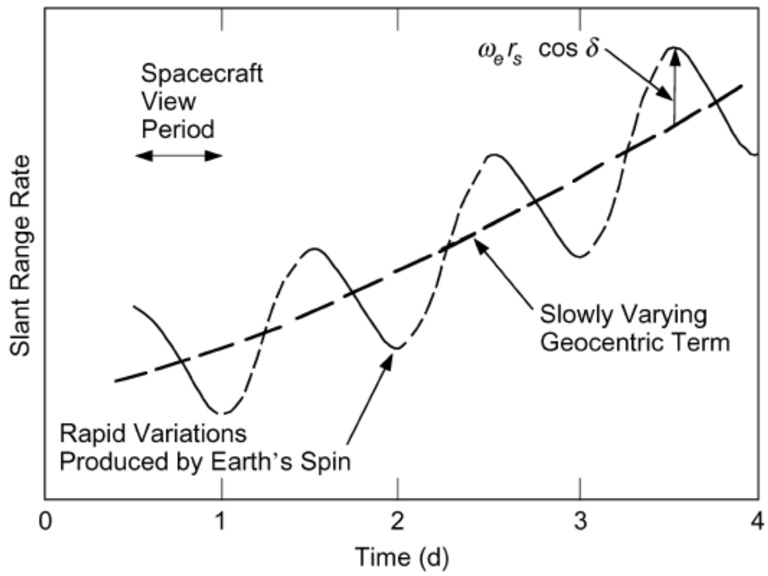

Figure 2 - Illustration of an idealized Doppler observable (from Ref 4).

Another way in which multiple DSN stations are used is to provide ΔDOR (delta differenced one-way range) measurements. Differenced one-way range (DOR) measurements take a one-way signal that is received at two different DSN stations, and determines the time-delay between the signal arrival at each station, as pictured on the left panel of Figure 3. This time difference is converted to a range, and combined with the known relative position of the two stations (the baseline), the angular position of the spacecraft can be constrained. Note that in the picture shown, there is no information constraining those vectors to lie in the page, so that θ is determined, but the position vectors could be rotated anywhere around the baseline. The problem with DOR measurements is that since the signal takes a different path through the atmosphere to each station, there can be significant errors that are difficult to calibrate out. This is resolved by differencing the DOR measurement from the spacecraft, with the time-delay between stations viewing the same quasar (right of Figure 3). If the quasar is located near the spacecraft in this sky, the signals from the quasar and the spacecraft follow similar paths through the atmosphere, and subtracting Δt_Q will remove the atmospheric differences. The result of this process is a very accurate measurement of the position of the spacecraft on the sky. Using two different baselines that are not parallel (such as Madrid-Goldstone and Goldstone-Canberra) can ensure full angular observability, and similar to range measurements, an arc of ΔDOR will also provide information on the angular rates.

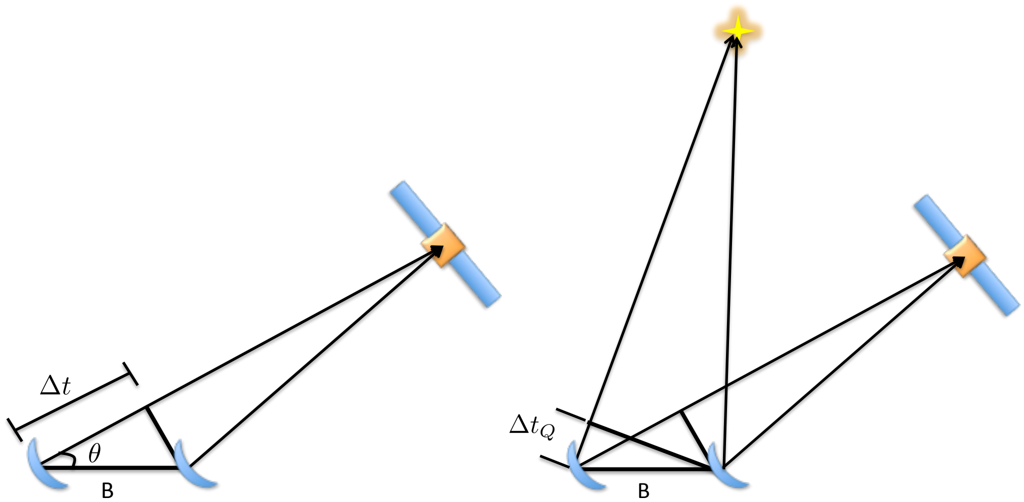

Figure 3 - Schematic of Delta-DOR measurements

Throughout the RS phases of the mission, we will also use measurements obtained from the optical cameras and LiDAR onboard the spacecraft. These are very powerful measurements as they measure aspects of the spacecraft's position *with respect to RQ36*. Without these relative measurements, we have no accurate information about RQ36's position, except as implied by the solution of the spacecraft state; the RQ36 ephemeris is accurate to ~10km, whereas our orbits around RQ36 are less than 1km. In order to accurately estimate parameters about RQ36, such as its spin state and gravity field, it will be necessary to use some relative navigation measurements.

Unlike the DSN data types, the RS team will obtain pre-processed versions of these measurements from the Image Processing (optical) and Altimetry (LiDAR) working groups, instead of the raw instrument data. Preferably the optical data will be pre-processed into unit (direction) vector measurements from the spacecraft to the center of RQ36, and the LiDAR data will be pre-processed to a set of distance measurements from the spacecraft to the center of RQ36. These measurements are illustrated in Figure 4. In each optical image, landmarks are identified to determine the spacecraft pointing with respect to RQ36. The LiDAR data measures the distance from the spacecraft to the surface of RQ36. This measurement can be related to the distance to the center of the asteroid by using the spacecraft pointing and the shape model of RQ36. Clearly the optical and LiDAR measurements are synergistic, and both give measurements relative to the asteroid that the DSN measurements can't directly provide. The precise determination of data from these groups is still to be finalized.

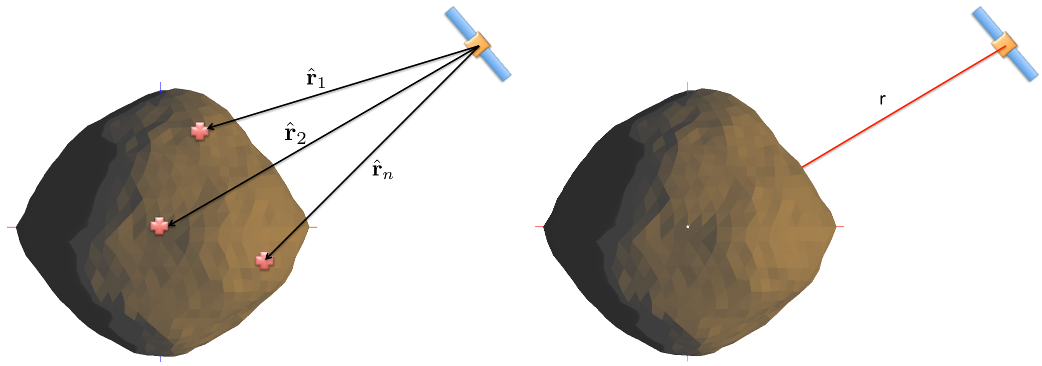

Figure 4 - Illustration of optical navigation measurements (left) and LiDAR range measurements (right).

Measurement Cadence:

The Design Reference Mission (DRM) defines the measurement cadence for the mission. Within this regard, the fundamental rule of thumb for RS is that more data is better in the long run, as it will allow for more detailed analysis and more accurate estimation. However, during the mission operations, we will use specific sets of measurement data in order to meet the Level 2 science requirements during the expected mission phases. The main phases for information gathering and initial delivery of RS products are the Survey (4), Orbital (5), and Reconnaissance (6) phases.

The initial portion of the survey phase, DRM phase 4A, is a crucial time for RS. There will be three slow fly-bys of RQ36, each lasting approximately 2 days, which will provide the data to get initial mass and center of mass estimates. During this phase, RS will use 8 hours per day of Doppler and ranging data, as well as 4 days with 1 hour of ΔDOR measurements. Optical and LiDAR measurements will also be taken around the closest approach of each fly-by.

Doppler and ranging data will continue to be taken at a rate of 8 hours a day during phase 4B, when the spacecraft is maneuvering to multiple different viewing orbits.

The key DSN measurements used to satisfy RS requirements occur during the orbital phase. The spacecraft will be in a 1.5km terminator orbit during phase 5A, and a significant amount of Doppler, ranging, optical, and LiDAR data will be taken. During phase 5B, the spacecraft moves to a 1km orbit. In this phase, there is a week where there will be continuous DSN coverage for 3-days (24 hours a day), 1 day with 8 hours of coverage, and then another 3-day continuous coverage period. This set of data is crucial to driving errors on all estimates as low as possible because during this time the spacecraft will be essentially quiescent, allowing for minimal perturbations to the natural dynamics.

Finally, the reconnaissance phase will put the spacecraft in 450m orbits, which will add significantly more information for determining the higher-order gravity field coefficients.

Data Products

The RS process will produce the following data products to satisfy the assigned requirements.

- An ASCII file containing the currently estimated RQ36 mass and center of mass location, along with associated errors. This will be used to satisfy requirements 2.8.2 and 2.8.4. This will be produced for all RS phases of the mission.
- An ASCII file containing the RQ36 gravity field information. A spherical harmonic gravity field will be included to at least 4th degree and order, along with associated errors, to satisfy requirement 2.8.3. A second gravity field representation will be used to give the surface gravity field and associated errors, to satisfy requirement 2.7.5. This will be produced for RS phases of the mission beginning in phase 5B.
- An ASCII file containing the currently estimated RQ36 rotation state with the associated errors. This file will include the rotation pole right ascension, declination, and obliquity, the rotation pole wobble, and the rotation period, along with all associated errors. This information will be used to satisfy requirements 2.7.2, 2.7.3, and 2.7.4. This will be produced for RS phases of the mission beginning in phase 4B.
- A SPICE kernel including the currently estimated state parameters. This file is not used to meet any requirements, but will allow for easy comparison with the Navigation team solution, as well as being used as the a priori estimate for future arcs of data. This will be produced for all RS phases of the mission, although the state will change as the mission progresses.

It should be noted here that the specific requirements may be met early in the RS mission, however the estimates will continue to be improved as much as possible using any and all available data. For example, the RQ36 mass will be determined to within 0.5% (as per requirement 2.8.2) during DRM phase 4A, however this estimate will be continuously improved as more measurements are made available during the mission around RQ36.

Covariance Analysis

The RS team has conducted extensive covariance analysis to ensure that the planned Data Acquisition Strategy will be sufficient for meeting the RS requirements. These analyses focus on the necessary information needed in terms of types of measurements, number of measurements, and accuracy of the measurements. Specific attention is paid to the role of the optical and LiDAR measurements in supplementing the DSN data types in order to meet the RS requirements. In the following, some results from the covariance studies are presented for the Survey and Orbital phases.

Survey Phase Analysis

This analysis analyzed how well the gravity field up to second degree and order, as well as the spin state of RQ36, can be determined from five fly-bys. While this is not the precise mission as the DRM is now planned, it indicates how well these parameters can be estimated from fly-bys. The measurements used during these fly-bys are given in Table 1.

Table 1 - Measurement information for fly-by analysis

Measurement Type	Interval/Time	Uncertainty
Doppler	Continual at 60 $[s]$ interval	0.1 $[mm/s]$
Earth Range	Continual at 1 $[hr]$ interval	10 $[m]$
Optical	Continual at 2.4 $[hr]$ interval	68 $[micro\ rad.]$
Lidar	Discrete at $[-1, 0, 1]$ $[hr]$ around the target point	10 $[m]$

The results of this analysis for a case with nominal density of RQ36 ($\rho = 0.98\ g/cm^3$) are shown in Table 2. The filter was run with and without the LiDAR data incorporated into the estimates, and three cases were run each way: only estimating the listed parameters; estimating the parameters and also considering the third and fourth degree gravity field; and smoothing the results, which should be the best in all cases. Note that results given as a ratio are the 1σ values divided by the true value.

Table 2 – 1σ uncertainties in estimated parameters for the fly-by analysis.

	Lidar On			Lidar Off		
	Regular	*Consider*	*Smoother*	*Regular*	*Consider*	*Smoother*
μ [ratio]	1.71595×10^{-4}	1.71756×10^{-4}	1.22124×10^{-4}	1.73131×10^{-4}	1.73290×10^{-4}	1.23241×10^{-4}
η [n.d.]	1.41298×10^{-3}	1.41340×10^{-3}	1.02617×10^{-3}	1.41311×10^{-3}	1.41354×10^{-3}	1.02637×10^{-3}
α [rad.]	5.66981×10^{-4}	5.67388×10^{-4}	4.02959×10^{-4}	5.69141×10^{-4}	5.69547×10^{-4}	4.04584×10^{-4}
β [rad.]	5.28341×10^{-5}	5.28556×10^{-5}	3.81900×10^{-5}	5.30820×10^{-5}	5.31036×10^{-5}	3.83816×10^{-5}
γ [rad.]	5.38249×10^{-4}	5.38684×10^{-4}	3.81988×10^{-4}	5.39227×10^{-4}	5.39662×10^{-4}	3.82743×10^{-4}
$\dot{\gamma}$ [rad./s]	6.09695×10^{-11}	6.09827×10^{-11}	4.34416×10^{-11}	6.25193×10^{-11}	6.25332×10^{-11}	4.45512×10^{-11}
$\mathbf{C_{1,0}}$ [n.d.]	3.51552×10^{-4}	3.51677×10^{-4}	2.50411×10^{-4}	3.51874×10^{-4}	3.51998×10^{-4}	2.50631×10^{-4}
$\mathbf{C_{1,1}}$ [n.d.]	7.84611×10^{-4}	7.85516×10^{-4}	5.53978×10^{-4}	7.85271×10^{-4}	7.86177×10^{-4}	5.54454×10^{-4}
$\mathbf{C_{2,0}}$ [n.d.]	1.31551×10^{-3}	1.31614×10^{-3}	9.38020×10^{-4}	1.32075×10^{-3}	1.32138×10^{-3}	9.41966×10^{-4}
[ratio]	3.83934×10^{-2}	3.84118×10^{-2}	2.73762×10^{-2}	3.85463×10^{-2}	3.85646×10^{-2}	2.74913×10^{-2}
$\mathbf{C_{2,1}}$ [n.d.]	1.04886×10^{-3}	1.05063×10^{-3}	7.50547×10^{-4}	1.04953×10^{-3}	1.05131×10^{-3}	7.51023×10^{-4}
$\mathbf{C_{2,2}}$ [n.d.]	1.73078×10^{-3}	1.73274×10^{-3}	1.22659×10^{-3}	1.73295×10^{-3}	1.73491×10^{-3}	1.22814×10^{-3}
[ratio]	5.01923×10^{-1}	5.02490×10^{-1}	3.55709×10^{-1}	5.02552×10^{-1}	5.03121×10^{-1}	3.56159×10^{-1}
$\mathbf{S_{1,1}}$ [n.d.]	1.09932×10^{-3}	1.09987×10^{-3}	7.76207×10^{-4}	1.09941×10^{-3}	1.09995×10^{-3}	7.76264×10^{-4}
$\mathbf{S_{2,1}}$ [n.d.]	9.21130×10^{-4}	9.23452×10^{-4}	6.59680×10^{-4}	9.22692×10^{-4}	9.25008×10^{-4}	6.60894×10^{-4}
$\mathbf{S_{2,2}}$ [n.d.]	1.91347×10^{-3}	1.91557×10^{-3}	1.35696×10^{-3}	1.91378×10^{-3}	1.91589×10^{-3}	1.35720×10^{-3}

The symbols are as follows: μ is the gravitational parameter; η is the solar radiation pressure scale factor; α, β, and γ are the orientation parameters for RQ36; $\dot{\gamma}$ is RQ36's spin rate; the C and S parameters are the gravity field coefficients.

The methodology for conducting this type of fly-by analysis is discussed in detail in Reference 2.

Orbital Phase Analysis

The orbital phase analysis looked at the case of the spacecraft in the 1.5km terminator orbit for four weeks, followed by one week in the 1km terminator orbit. These orbits are pictured in Figure 5. Over the 4 week period, the 1.5km orbit drifts from the red shape to the yellow shape as shown. The blue line in the 1km figure shows the propagation of the estimated orbit for 2 days after data cutoff.

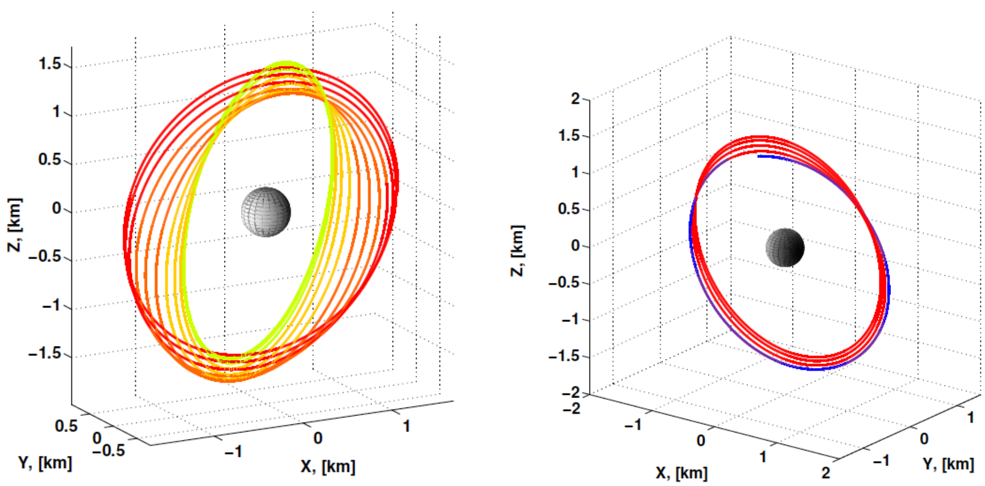

Figure 5 - The 1.5 (left) and 1km terminator orbits.

The 1.5km orbit had the measurements shown in Table 3, and the 1km measurements are in Table 4.

Table 3 - Measurements used for 1.5km orbit

Measurement Type	Interval/Time	Uncertainty
Doppler	Continual at 60 $[s]$ interval for the first 8 $[hrs]$ each day and repeating	0.1 $[mm/s]$
Earth Range	Continual at 1 $[hr]$ interval	10 $[m]$
Optical	Continual at 2.4 $[hr]$ interval	68 $[micro\ rad.]$
Lidar	Continual at 0.5 $[hr]$ interval	10 $[m]$

Table 4 - Measurements used for 1km orbit

Measurement Type	Interval/Time	Uncertainty
Doppler	Continual at 60 $[s]$ interval	0.1 $[mm/s]$
Earth Range	Continual at 1 $[hr]$ interval	10 $[m]$
Optical	Continual at 2.4 $[hr]$ interval	68 $[micro\ rad.]$
Lidar	Continual at 0.5 $[hr]$ interval	10 $[m]$

This analysis looked at estimating the gravity field up to 4th order, while considering 5th and 6th orders. Here we show the results for the case with the nominal RQ36 density, although 3σ high- and low-density cases were also analyzed. The estimation uncertainties are shown in Table 5. Note that in this case, the gravity coefficients are normalized, as opposed to the fly-by case discussed above.

Table 5 - Uncertainties for orbital phase estimation after the 1km orbit

	Lidar On			Lidar Off		
	Regular	*Consider*	*Smoother*	*Regular*	*Consider*	*Smoother*
μ [ratio]	8.68913×10^{-5}	8.68913×10^{-5}	6.15034×10^{-5}	8.71429×10^{-5}	8.71429×10^{-5}	6.16822×10^{-5}
η [n.d.]	2.15283×10^{-4}	2.15283×10^{-4}	1.52539×10^{-4}	2.15503×10^{-4}	2.15503×10^{-4}	1.52696×10^{-4}
α [rad.]	9.34579×10^{-6}	9.34579×10^{-6}	6.68271×10^{-6}	9.34623×10^{-6}	9.34623×10^{-6}	6.68305×10^{-6}
β [rad.]	2.99526×10^{-5}	2.99526×10^{-5}	2.20626×10^{-5}	2.99646×10^{-5}	2.99646×10^{-5}	2.20721×10^{-5}
γ [rad.]	9.45965×10^{-6}	9.45965×10^{-6}	6.90634×10^{-6}	9.46144×10^{-6}	9.46144×10^{-6}	6.90778×10^{-6}
$\dot{\gamma}$ [rad./s]	2.45035×10^{-11}	2.45035×10^{-11}	1.78135×10^{-11}	2.45077×10^{-11}	2.45077×10^{-11}	1.78169×10^{-11}
$\bar{C}_{1,0}$ [n.d.]	2.19729×10^{-4}	2.19729×10^{-4}	1.55429×10^{-4}	2.20117×10^{-4}	2.20117×10^{-4}	1.55704×10^{-4}
$\bar{C}_{1,1}$ [n.d.]	9.14264×10^{-4}	9.14264×10^{-4}	6.47541×10^{-4}	9.14281×10^{-4}	9.14281×10^{-4}	6.47553×10^{-4}
$\bar{C}_{2,0}$ [n.d.]	7.34663×10^{-4}	7.34663×10^{-4}	5.23910×10^{-4}	7.34792×10^{-4}	7.34792×10^{-4}	5.23998×10^{-4}
[ratio]	4.79440×10^{-2}	4.79440×10^{-2}	3.41903×10^{-2}	4.79524×10^{-2}	4.79524×10^{-2}	3.41960×10^{-2}
$\bar{C}_{2,1}$ [n.d.]	2.93802×10^{-3}	2.93802×10^{-3}	2.09529×10^{-3}	2.93808×10^{-3}	2.93808×10^{-3}	2.09534×10^{-3}
$\bar{C}_{2,2}$ [n.d.]	7.61222×10^{-3}	7.61222×10^{-3}	5.48723×10^{-3}	7.61225×10^{-3}	7.61225×10^{-3}	5.48725×10^{-3}
$\bar{C}_{3,0}$ [n.d.]	8.96886×10^{-4}	8.96896×10^{-4}	6.39792×10^{-4}	8.97381×10^{-4}	8.97392×10^{-4}	6.40136×10^{-4}
$\bar{C}_{3,1}$ [n.d.]	1.02086×10^{-2}	1.02086×10^{-2}	7.55804×10^{-3}	1.02089×10^{-2}	1.02089×10^{-2}	7.55823×10^{-3}
$\bar{C}_{3,2}$ [n.d.]	2.17443×10^{-2}	2.17443×10^{-2}	1.78047×10^{-2}	2.17443×10^{-2}	2.17443×10^{-2}	1.78048×10^{-2}
$\bar{C}_{3,3}$ [n.d.]	2.66610×10^{-2}	2.66610×10^{-2}	2.39154×10^{-2}	2.66610×10^{-2}	2.66610×10^{-2}	2.39154×10^{-2}
$\bar{C}_{4,0}$ [n.d.]	1.39493×10^{-2}	1.39493×10^{-2}	1.06052×10^{-2}	1.39512×10^{-2}	1.39512×10^{-2}	1.06070×10^{-2}
$\bar{C}_{4,1}$ [n.d.]	2.45173×10^{-2}	2.45173×10^{-2}	2.10950×10^{-2}	2.45177×10^{-2}	2.45177×10^{-2}	2.10955×10^{-2}
$\bar{C}_{4,2}$ [n.d.]	2.98193×10^{-2}	2.98193×10^{-2}	2.90771×10^{-2}	2.98193×10^{-2}	2.98193×10^{-2}	2.90771×10^{-2}
$\bar{C}_{4,3}$ [n.d.]	3.03920×10^{-2}	3.03920×10^{-2}	3.01470×10^{-2}	3.03920×10^{-2}	3.03920×10^{-2}	3.01470×10^{-2}
$\bar{C}_{4,4}$ [n.d.]	3.05299×10^{-2}	3.05299×10^{-2}	3.04145×10^{-2}	3.05299×10^{-2}	3.05299×10^{-2}	3.04145×10^{-2}
$\bar{S}_{1,1}$ [n.d.]	9.21170×10^{-4}	9.21170×10^{-4}	6.52510×10^{-4}	9.21188×10^{-4}	9.21188×10^{-4}	6.52523×10^{-4}
$\bar{S}_{2,1}$ [n.d.]	2.95369×10^{-3}	2.95369×10^{-3}	2.10597×10^{-3}	2.95375×10^{-3}	2.95375×10^{-3}	2.10601×10^{-3}
$\bar{S}_{2,2}$ [n.d.]	7.62127×10^{-3}	7.62127×10^{-3}	5.49493×10^{-3}	7.62131×10^{-3}	7.62131×10^{-3}	5.49495×10^{-3}
$\bar{S}_{3,1}$ [n.d.]	1.02355×10^{-2}	1.02355×10^{-2}	7.58462×10^{-3}	1.02357×10^{-2}	1.02357×10^{-2}	7.58480×10^{-3}
$\bar{S}_{3,2}$ [n.d.]	2.16887×10^{-2}	2.16887×10^{-2}	1.77510×10^{-2}	2.16887×10^{-2}	2.16887×10^{-2}	1.77510×10^{-2}
$\bar{S}_{3,3}$ [n.d.]	2.66457×10^{-2}	2.66457×10^{-2}	2.38931×10^{-2}	2.66457×10^{-2}	2.66457×10^{-2}	2.38931×10^{-2}
$\bar{S}_{4,1}$ [n.d.]	2.43364×10^{-2}	2.43364×10^{-2}	2.09713×10^{-2}	2.43368×10^{-2}	2.43368×10^{-2}	2.09718×10^{-2}
$\bar{S}_{4,2}$ [n.d.]	2.98105×10^{-2}	2.98105×10^{-2}	2.90629×10^{-2}	2.98105×10^{-2}	2.98105×10^{-2}	2.90629×10^{-2}
$\bar{S}_{4,3}$ [n.d.]	3.03925×10^{-2}	3.03925×10^{-2}	3.01478×10^{-2}	3.03925×10^{-2}	3.03925×10^{-2}	3.01478×10^{-2}
$\bar{S}_{4,4}$ [n.d.]	3.05299×10^{-2}	3.05299×10^{-2}	3.04145×10^{-2}	3.05299×10^{-2}	3.05299×10^{-2}	3.04145×10^{-2}

A similar study was conducted using GEODYN (Reference 3), which also showed that the gravity field could be determined to 4th degree and order. This study emphasized the importance of estimating the SRP force acting on the spacecraft, as well as the necessity of including optical measurements in order to estimate this gravity field.

References

1. McMahon, Jay, "GEODYN Usage for the OSIRIS-REx Radio Science Team," June 2012
2. Takahashi, Yu and Scheeres, Daniel, "Small-Body Postrendezvous Characterization via Slow Hyperbolic Flybys," Journal of Guidance, Control, and Dynamics, Vol. 34, No. 6, November-December 2011

3. Rowlands, Dave, *personal communication*, March 10, 2011
4. Thorton, Catherine and Border, James, Radiometric Tracking Techniques for Deep-Space Navigation, JPL Publication 00-11, October 2000